Transport in doped skutterudites: *Ab initio* electronic structure calculations

L. Chaput,[1] P. Pécheur,[1] J. Tobola,[2] and H. Scherrer[1]
[1]*Laboratoire de Physique des Matériaux, UMR 75560, ENSMN, Parc de Saurupt, 54042 Nancy, France*
[2]*Faculty of Physics and Applied Computer Science, AGH University of Science and Technology, Aleja Mickiewicza 30, 30-059 Cracow, Poland*

(Received 17 July 2004; revised manuscript received 24 May 2005; published 19 August 2005)

We present *ab initio* calculations of conductivity, thermopower, Lorenz factor, and Hall coefficient for doped cobalt antimony skutterudites which are currently investigated experimentally for their thermoelectric properties. The electronic structure is calculated by the full potential linear augmented-plane-wave method. Using the results and shifting the Fermi level in a rigid way to mimic doping, Onsager coefficients are calculated in the framework of Boltzmann transport theory with a constant relaxation time. To this end electron velocities are calculated using a spectral collocation method. These results compare favorably with experiments.

DOI: 10.1103/PhysRevB.72.085126 PACS number(s): 72.20.Pa, 72.10.Bg, 71.15.Mb

I. INTRODUCTION

Cobalt antimony skutterudites form a class of compounds which are extensively studied for their thermoelectric properties.[1] These compounds fall in the space group $Im3$ with cobalt and antimony atoms sitting on the $(8c)$ and $(24g)$ positions, respectively. It is well known that this structure can be described either as $CoSb_6$ octahedra sharing corners (see Fig. 1) or more commonly as a cubic array of cobalt atoms containing four-membered square planar rings of antimony atoms.

The thermoelectric figure of merit

$$Z = \frac{S^2\sigma}{\kappa} \tag{1}$$

(where σ is the electrical conductivity, S the Seebeck coefficient, and κ the thermal conductivity) measures the efficiency of a compound used in thermoelectric generators. It was found that cobalt antimony skutterudites have conductivity and thermopower quite favorable to achieve a high power factor σS^2, but unfortunately the thermal conductivity is too high to obtain a figure of merit suitable for applications.[2]

Many attempts have been undertaken to lower the thermal conductivity by doping following the concept of the phonon glass electron crystal (PGEC) proposed by Slack.[3] One way is to insert filling atoms in the large voids characteristic of the skutterudite structure (Fig. 1). These can be rare-earth atoms,[4,5] Ba, or Ca.[6–8] The filling atoms rattle in the voids and can then be seen as Einstein oscillators that scatter lattice phonons. This leads to a strong decrease in the thermal conductivity as demonstrated by Nolas *et al.*[4] Substitutional doping has also been performed, on either the cobalt or antimony site. The thermal conductivity is also reduced but the scattering mechanism is different.[9]

The doping is often performed with atoms that are close in atomic number to those of the pure matrix to ensure chemical stability. For example one can substitute Fe or Ni on the Co site. In these cases the rigid-band approximation is reasonable for the electronic structure. It may also be reasonable in the vicinity of the Fermi level when rare-earth elements are inserted in the voids since they do not hybridize strongly with the host lattice. This will be discussed in Sec. III. Using the rigid-band approximation, the conductivity tensor, thermopower, Lorenz factor, and Hall coefficient can be calculated for doped cobalt antimony skutterudites using the band structure of the host lattice. This is the purpose of the present work.

The paper is organized as follows. Based on the WIEN2K program[10] a FORTRAN *module* has been written to calculate transport coefficients. Details of the implementation are given in Sec. II and the Appendix. In Sec. III the electronic structure is discussed together with the rigid-band approxi-

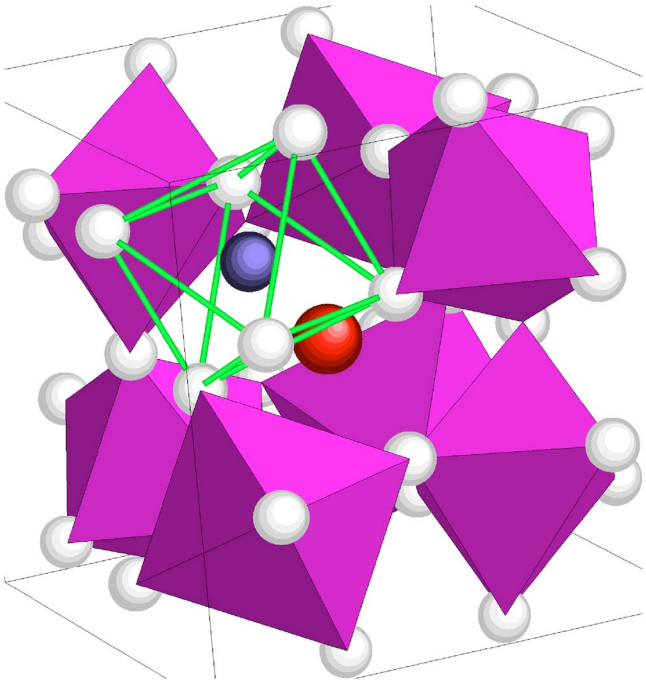

FIG. 1. (Color online) The filled skutterudite structure. Antimony atoms (white) are at the corners of octahedrons. Cobalt atoms (in blue) are inside Antimony octahedrons. The filling atom is at the center of the cell (red).

 ©2005 The American Physical Society

mation. The transport properties are calculated in Sec. IV and compared with experiments.

II. THEORY

In transport measurements quantities of interest are the electrical conductivity σ, thermopower S, electrical thermal conductivity κ_e, and Hall coefficient R_H:[11,12]

$$\sigma = L_{11}, \tag{2}$$

$$S = \frac{L_{11}^{-1} L_{12}}{T}, \tag{3}$$

$$\kappa_e = \frac{1}{T}\left(L_{22} - \frac{L_{21}L_{12}}{L_{11}}\right), \tag{4}$$

$$R_H = \frac{\rho_{yx}}{B}, \tag{5}$$

where L_{ij} are the Onsager coefficients defined through the electrical and heat current density $\vec{j}$ and $\vec{j}^{Q}$ [Eqs. (9) and (10)]. The evaluation of these quantities from first-principles calculations is based on a microscopic model for the system response to the applied fields $\vec{E}$, $\vec{\nabla} T$, and $\vec{B}$. In this paper we limit our considerations to the Boltzmann transport theory in the constant-relaxation-time approximation. The one-particle phase space distribution f is then obtained from the following equation:

$$\vec{v_k} \cdot \vec{\nabla} T \frac{\partial f}{\partial T} + \frac{q}{\hbar}(\vec{E} + \vec{v_k} \times \vec{B}) \cdot \frac{\partial f}{\partial \vec{k}} = -\frac{f - f_0}{\tau}, \tag{6}$$

where f_0 is the Fermi-Dirac distribution.

Once this equation is linearized [see Eq. (7)], the one-particle distribution can be written in terms of the vector mean free path $\vec{\Lambda}_k$ which is calculated in solving the Boltzmann equation [Eq. (6)],

$$f = f_0 - \left(q\vec{E} - \frac{\nabla T}{T}(\varepsilon_k - \mu)\right)\frac{\partial f_0}{\partial \varepsilon} \cdot \vec{\Lambda}_k. \tag{7}$$

If the electric field and temperature gradient are acting on the sample (without magnetic field), which corresponds to the conditions of conductivity and thermopower measurements, the Boltzmann equation can be easily solved and the vector mean free path $\vec{\Lambda}_k$ is simply given by

$$\vec{\Lambda}_k = \tau \vec{v}_k. \tag{8}$$

Then it is straightforward to obtain a microscopic expression for the Onsager coefficients in terms of the electrons velocities,

$$\vec{j} = \frac{1}{V}\sum_k q\vec{v}_k f_k = \left(\int d\varepsilon\, \sigma(\varepsilon)\frac{\partial f_0}{\partial \mu}\right)\vec{E} + \left(\int d\varepsilon \frac{1}{q}\sigma(\varepsilon)(\varepsilon - \mu)\frac{\partial f_0}{\partial \mu}\right)\left(-\frac{\nabla T}{T}\right),$$

$$\vec{j} = L_{11}\vec{E} + L_{12}\left(-\frac{\nabla T}{T}\right) \tag{9}$$

and

$$\vec{j}^{Q} = \frac{1}{V}\sum_k (\varepsilon_k - \mu)\vec{v}_k f_k = \left(\int d\varepsilon \frac{1}{q}\sigma(\varepsilon)(\varepsilon - \mu)\frac{\partial f_0}{\partial \mu}\right)\vec{E} + \left(\int d\varepsilon \frac{1}{q^2}\sigma(\varepsilon)(\varepsilon - \mu)^2 \frac{\partial f_0}{\partial \mu}\right)\left(-\frac{\nabla T}{T}\right),$$

$$\vec{j}^{Q} = L_{21}\vec{E} + L_{22}\left(-\frac{\nabla T}{T}\right), \tag{10}$$

where

$$\sigma(\varepsilon) = \frac{q^2\tau}{V}\sum_k \vec{v}_k \vec{v}_k \delta(\varepsilon_k - \varepsilon)$$

is the transport function.[13] In practice this is the quantity to be evaluated since it contains all necessary information about the system.

In Hall measurements, where the fields $\vec{E}$ and $\vec{B}$ are applied to the system, the vector mean free path cannot be written in a closed form as in Eq. (8). The Boltzmann equation is then rewritten in terms of the vector mean free path,

$$\vec{\Lambda}_k = \tau\vec{v}_k - \frac{q\tau}{\hbar}\left(\vec{v}_k \times \vec{B} \cdot \frac{\partial}{\partial \vec{k}}\right)\vec{\Lambda}_k, \tag{11}$$

and solved iteratively.

Once we have an approximate solution, the current density can be calculated and the conductivity tensor is expressed as a magnetic-field-dependent quantity:

$$\vec{j} = \frac{1}{V}\sum_k q\vec{v}_k f_k = \left(\int d\varepsilon \sigma_B(\varepsilon)\frac{\partial f_0}{\partial \mu}\right)\vec{E} = \sigma(\vec{B})\vec{E},$$

where

$$\sigma_B(\varepsilon) = \frac{q^2}{V}\sum_k \vec{v}_k \vec{\Lambda}_k \delta(\varepsilon_k - \varepsilon)$$

is the magnetic transport function. The Hall coefficient is then calculated from Eq. (5) using $\rho = \sigma^{-1}$.

In practice, integrals over the first Brillouin zone, $(1/V)\Sigma_k$, are evaluated using the tetrahedron method. Electron velocities, defined through the relation $\vec{v}_k = (1/\hbar)\nabla_k \varepsilon_k$, also need to be calculated. The usual methods for numerical differentiation, like finite differences, are not suitable since the velocities are to be calculated accurately, which would be very time consuming. Instead we used a spectral collocation method which is known for its accuracy. Roughly speaking this means that the convergence rate is exponential which reduces significantly the computational time. Details can be found in the book by Trefethen[14] and in the Appendix. The Hall coefficient is closely related to the curvature of the Fermi surface[15] which must be obtained with sufficient precision. The present implementation has been checked against previous calculations by Schulz *et al.*[16] for cubic metals, and good agreement was found.

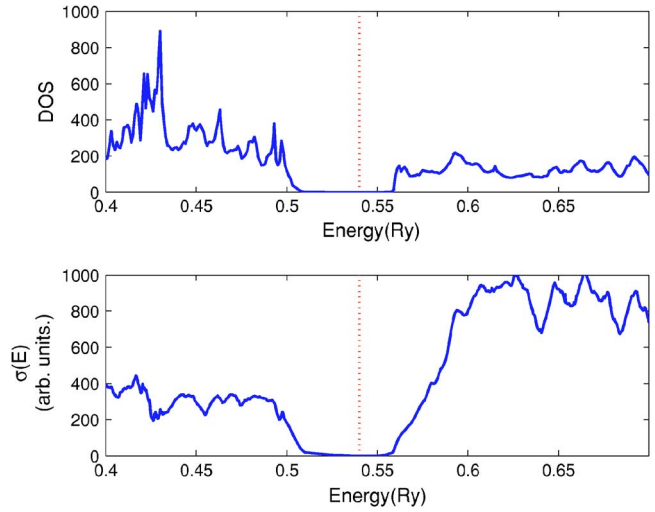

FIG. 2. (Color online) DOS and transport function in $CoSb_3$ skutterudites.

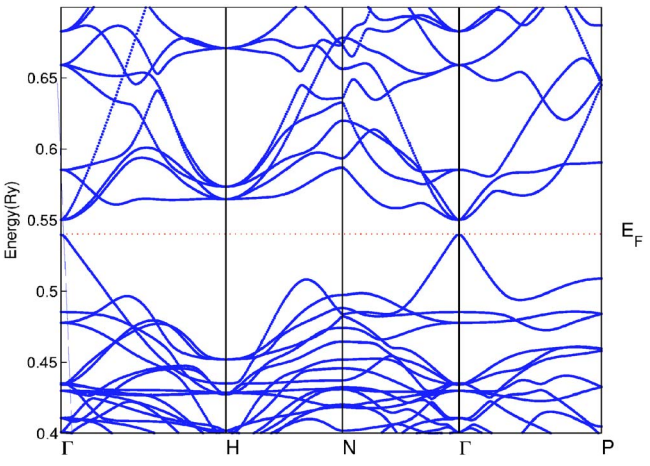

FIG. 3. (Color online) The $CoSb_3$ band structure around E_F.

III. ELECTRONIC STRUCTURE AND RIGID-BAND APPROXIMATION

Electronic structure calculations are performed in the framework of density functional theory using the full-potential linear augmented-plane-wave (FLAPW) method.[10] The exchange correlation part of the potential is calculated in a generalized gradient approximation with the functional form proposed by Perdew *et al.*[17] Nonspherical terms in the potential up to $l=4$ are included during the self-consistency cycle which is realized with 2000 k points in the first Brillouin zone. The unit cell (Fig. 1) is divided into core and interstitial regions by muffin-tin spheres, with radius $R=2.35$ a.u. for the cobalt and antimony atoms. The value of Rk_{max} is fixed to 7.0 and the Fourier expansions are calculated up to $G_{max}=14$. The spin-orbit (SO) coupling was not included in the present work. It is noteworthy that the SO interactions were taken into account by Singh and Pickett[18] in the FLAPW calculations of $IrSb_3$ and rather minor effect on the band dispersion was found. Very recently, Koga *et al.*[19] have also performed FLAPW electronic structure calculations in MSb_3 (M=Co, Rh, and Ir) including the SO coupling. This effect is rather small (23 meV) in $CoSb_3$ at the Γ point but it may influence the transport properties at very small concentration doping. Since we are mostly interested in heavily doped $CoSb_3$ skutterudites with the Fermi level lying well above the conduction-band edge, we expect that the SO coupling cannot affect the electron transport coefficient calculations of the investigated systems.

The $CoSb_3$ electronic structure we found (Figs. 2 and 3) is almost identical to those previously reported in the literature[18,20,21] and the band gap is around 0.14 eV, in good agreement with the value recently calculated in Ref. 21. The authors in Refs. 18–20 calculated the E_g value of 0.05, 0.22, and 0.118 eV, respectively. The band-gap value is strongly dependent on the hybridization between p states of antimony atoms which form planar rings. This explains (together with the use of different exchange-correlation functionals) the range of E_g values reported in the literature. In our calculation we used the lattice constant and atomic positions from Ref. 22, namely, $a=9.0385$ Å and $(0,u,v)$ for Sb($24g$) sites with $u=0.3351$ and $v=0.1602$. Since the bands themselves change only a little, the effect on transport properties of heavily doped skutterudites (which is the case we consider in the present work) is rather small (see Fig. 12).

We now discuss the rigid-band approximation that is used in the next section for the calculation of transport properties. Since transport properties involve only electronic states around the Fermi level, this approximation is reasonable if the electronic structure of the bare $CoSb_3$ skutterudite does not change substantially around E_F under doping. We prove the validity of this assumption in two examples that will be discussed in Sec. IV.

First we consider the substitution of cobalt by iron and nickel. We have performed self-consistent Korringa-Kohn-Rostoker calculations with the coherent potential approximation (KKR-CPA),[23–25] since the FLAPW WIEN2K code does not allow one to treat disorder. The densities of states (DOSs) are presented in Fig. 4. We can see that, as expected, the DOS does not change much around E_F.

Next we consider the case of cobalt antimony skutterudites doped with neodymium atoms. The Nd atoms go in the voids (see Fig. 1). For such f-state elements, one cannot expect the local density approximation (LDA) computations to give reasonable results. So the electronic structure for $NdCo_4Sb_{12}$ has been calculated in the LDA+U framework with the method proposed by Anisimov *et al.*[26] The WIEN2K implementation[27] was used with Hubbard parameter $U=0.4$ Ry and exchange interaction $J=0.07$ Ry similar to those used in Ref. 28 for Pr. The density of states is shown in Fig. 5. Nd is found in a 3+ state with spin-up f states well above the gap. For spin-down states there are two groups of f bands separated by 0.45 Ry. The upper bands are located around 0.07 Ry above the band gap and the lower bands well below the band gap. We have also performed calculations employing other U parameters, namely, 0.3, 0.5, and 0.6 Ry. In each case the upper bands stay far above the band gap. If we assume that this picture is still valid for partly filled skutterudites $Nd_xCo_4Sb_{12}$ ($x<1$), the rigid-band approximation for the calculations of transport coefficients is satisfactory since the DOS is not perturbed in the vicinity of the gap.

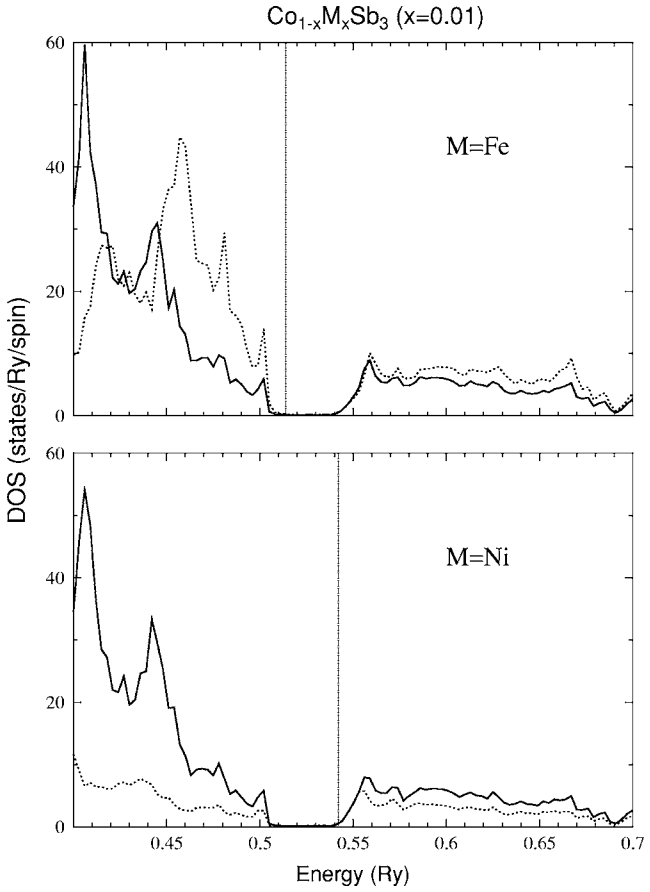

FIG. 4. $CoSb_3$ skutterudites doped on Co site. The solid line shows the total DOS and the dotted line is for the doping atom. The calculations were performed by the KKR-CPA and the parameters used are the same as in Ref. 23.

This conclusion should not be altered even when accounting for spin-orbit coupling since f states are expected to remain far from the conduction band edge.

IV. RESULTS

In this section we present the calculation of the transport coefficients, the Hall coefficient R_H and the Lorenz factor L and next the thermopower S and conductivity σ. All these calculations have been performed with 30 000 k points in the first Brillouin zone. The convergence has been checked against calculations with 10 000 k points. Note that since a constant value of τ has been used it does not appear in S, L, and R_H which are given by ratio of L_{ij}.

A. Hall coefficient

We first discuss the calculation of the Hall coefficient according to Eq. (5). The mean free path is obtained from Eq. (11) iterated only once (weak-field limit). Our calculation is then equivalent to the Ziman's formula[11] where R_H is independent of B and τ.

In transport measurements the carrier concentration n is frequently deduced from R_H using the free-electron formula

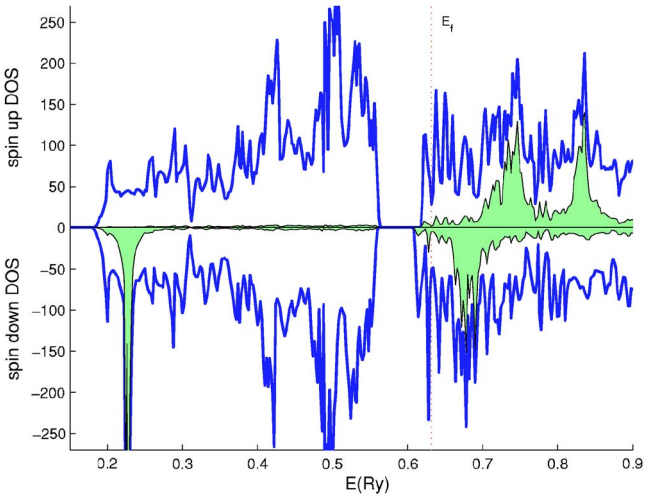

FIG. 5. (Color online) $NdCo_4Sb_{12}$ density of states. Total spin-projected DOSs are shown solid (blue) and f states are shadowed (green).

$$R_H = \frac{1}{nq}. \tag{12}$$

In order to see if Eq. (12) can be directly used in real skutterudite materials we have analyzed the theoretical Hall number n_H deduced from the R_H calculations as a function of the carrier concentration n according to the expression

$$n_H \equiv \frac{1}{R_H q} = \alpha(n) n, \tag{13}$$

where the coefficient $\alpha(n)$ can depend on the doping concentration n. In Fig. 6 the dotted curves (in black) correspond to the free-electron case $n_H = \alpha n$ (with $\alpha \pm 1$).

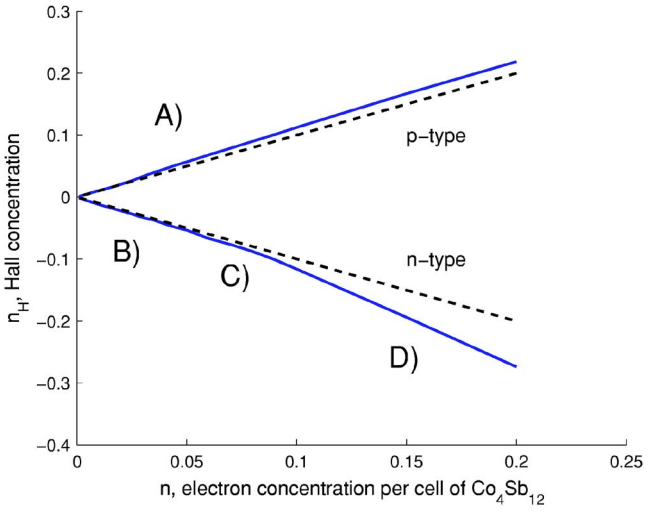

FIG. 6. (Color online) Calculated Hall number as a function of the electron doping concentration [solid (blue) line]. The Hall number n_H is calculated according to $n_H = 1/qR_H$ with R_H from Eq. (5) for different electron concentrations n. The regions A, B, C, and D correspond to the Fermi surface shapes shown in Fig. 7. The dotted (black) curves compare the free-electron formula.

In general, at low doping concentration the constant-energy surfaces $\epsilon(k)=\epsilon$ are roughly ellipsoidal and centered in Γ. The Hall number is then almost equal to n (α close to ± 1; see Ref. 29) for both p- and n-type doping. We expect that this conclusion should be also valid when the bands at Γ are split upon the SO inclusion, since contributions coming from different bands are weighted and again falls to $\alpha \approx 1$.

Furthermore, for heavy p doping the constant-energy surfaces of the valence band are still nearly ellipsoidal [see Fig. 7(a) where $n \sim 0.01$ hole and $E_F \sim 0.519$ Ry] and the calculated coefficient α is therefore also close to 1 ($\alpha = +1.1$ in our calculation). On the other hand, for the conduction band we can roughly distinguish two slopes in Fig. 6 (regions B and D). For $n < 0.06$ the slope is $\alpha = -1.1$ whereas α is around -1.6 for $n > 0.08$. For the intermediate concentrations (region C in Fig. 6) α depends on the concentration n due to the marked change of the Fermi surface topology. Figure 3 shows that three bands cross the Fermi level in this range of concentration ($E_F \lesssim 0.56$ Ry). All of them have been taken into account in the calculations of R_H. Two of these bands have constant-energy surfaces which are centered in Γ and remain nearly ellipsoidal over all the range of doping investigated in Fig. 6. The surface of constant energy corresponding to the third band is represented in Figs. 7(b)–7(d), respectively, for $n \sim 0.01$, $n \sim 0.06$, and $n \sim 0.09$ electrons per cell, respectively. Clearly, there is a change of topology responsible for the change of slope observed in Fig. 6. The pockets in Fig. 7(c) do not have very large curvature and therefore α is still not very different from -1. We observe in Fig. 7(d) that for higher n concentration these pockets become connected. This topological change seems to be mainly responsible for the α change between $n = 0.06$ and 0.08.

In our calculations of the Hall coefficient we have not taken into account the contributions to α coming from the dependence of τ with energy (since we use a constant τ_0) but this contribution is not expected to be large (see Ref. 29) and α remains close to 1.

B. Lorenz factor

The outputs of band structure calculations are now used to calculate the Lorenz factor but first we look at the transport distribution since it contains all the relevant information for transport properties (Fig. 2).

For a heavily doped semiconductor where the chemical potential is deep inside the conduction (or valence) band and

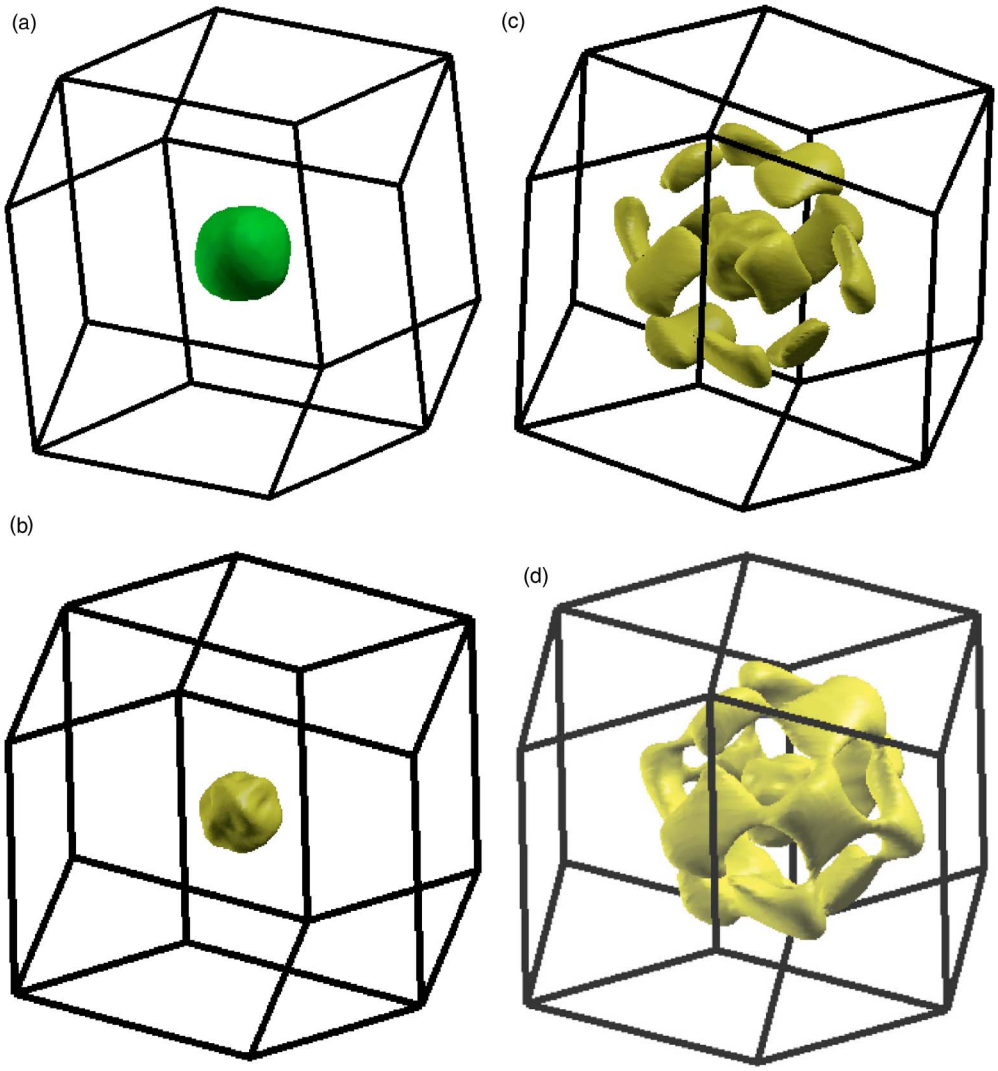

FIG. 7. (Color online) Fermi surface at various doping concentration (see Fig. 6). (a) corresponds to $n \sim 0.01$ holes and $E_F \sim 0.519$ Ry. (b), (c), and (d) we have $n \sim 0.01$, 0.06, and 0.09 electrons and $E_F \sim 0.5570$, 0.5591, and 0.5595 Ry, respectively.

since $(-\partial f_0/\partial\varepsilon)$ is very sharp, the integrals in Eqs. (9) and (10) can be calculated using[12]

$$\sigma(\epsilon) = a_\mu(\varepsilon - \mu) + b_\mu.$$

Then in the metallic approximation, the Onsager coefficients are easily found to be

$$L_{11} = b_\mu, \tag{14}$$

$$L_{12} = \frac{\pi^2}{3}(k_B T)^2 a_\mu, \tag{15}$$

$$L_{22} = \frac{\pi^2}{3}(k_B T)^2 b_\mu. \tag{16}$$

However, when the chemical potential lies within the band gap this metallic approximation is no longer valid but in this case the Fermi-Dirac distribution can be replaced by the Maxwell-Boltzmann function. Then Eqs. (9) and (10) can be calculated using

$$\sigma(\varepsilon) = \begin{cases} a_1\left(\varepsilon + \dfrac{\varepsilon_g}{2}\right) & \text{if } \varepsilon < -\dfrac{\varepsilon_g}{2}, \\ a_2\left(\varepsilon - \dfrac{\varepsilon_g}{2}\right) & \text{if } \varepsilon > \dfrac{\varepsilon_g}{2}, \end{cases}$$

since the integrals are dominated by the band edge contributions. The Onsager coefficients can then be expressed as

$$\begin{aligned} L_{ij} = {} & \frac{a_2}{\beta^{i+j-1}} e^{-\beta(\varepsilon_g/2-\mu)} \left\{ \left[\beta\left(\frac{\varepsilon_g}{2} - \mu\right)\right]^{i+j-1} - (i+j-2)! \right. \\ & \left. \times \left[\beta\left(\frac{\varepsilon_g}{2} - \mu\right) - (i+j-1)\right] e_{i+j-1}\left[\beta\left(\frac{\varepsilon_g}{2} - \mu\right)\right] \right\} \\ & + \frac{a_1(-1)^{i+j-1}}{\beta^{i+j-1}} e^{-\beta(\varepsilon_g/2+\mu)} \left\{ \left[\beta\left(\frac{\varepsilon_g}{2} - \mu\right)\right]^{i+j-1} - (i+j \right. \\ & \left. - 2)! \left[\beta\left(\frac{\varepsilon_g}{2} + \mu\right) - (i+j-1)\right] e_{i+j-1}\left[\beta\left(\frac{\varepsilon_g}{2} + \mu\right)\right] \right\}, \end{aligned} \tag{17}$$

where $e_\nu(x) = \sum_{k=0}^{\nu-1} x^k/k!$ is the exponential sum function.

This expression can be then used to calculate the Lorenz factor according to

$$L = \frac{\kappa_e}{T\sigma} = \frac{1}{T}\frac{L_{22} - L_{21}(L_{11})^{-1}L_{12}}{L_{11}}. \tag{18}$$

For a transport distribution $\sigma(E)$ as in Fig. 8(a) we get the curve shown in Fig. 8(b) for the Lorenz factor. For very heavy doping where the chemical potential is deep inside the valence or conduction band the Lorenz factor takes the metallic limit $L = L_0 = (\pi^2/3)k_B^2/e^2$. However, at intermediate doping concentration L is smaller than L_0 and then passes by a minimum to become larger than L_0 at very small doping concentration. This behavior $(L \neq L_0)$ can have some consequences for the determination of the thermal conductivity. The Lorenz factor is generally used to separate the electronic (κ_e) and lattice (κ_L) contributions to the thermal conductivity

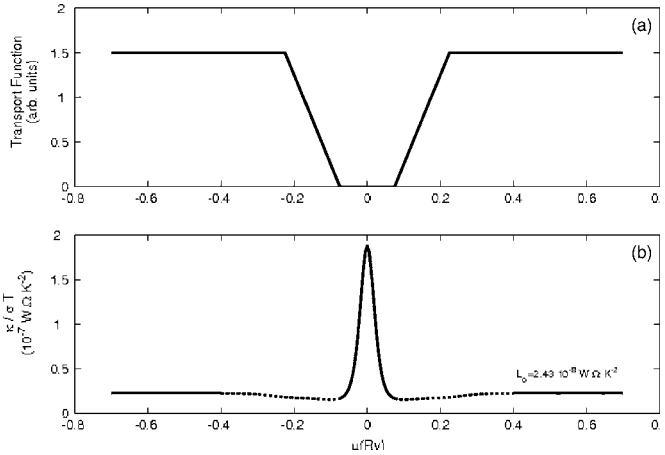

FIG. 8. The transport distribution (a) and the Lorenz factor (b) at 300 K.

$\kappa = \kappa_L + \kappa_e$, since following the Wiedemann-Franz law $\kappa_e = L_0\sigma T$ the electronic contribution κ_e can be extracted from the electrical conductivity measurements σ. As we have seen in Fig. 8 the value for the Lorenz factor can be substantially different from L_0 at intermediate and low doping concentration, and therefore may lead to a wrong estimation for the electronic and lattice thermal conductivity.

To see what difference between L and L_0 can be expected in doped $CoSb_3$ skutterudites we used the computed electronic structure to calculate the Lorenz factor [Eq. (18)]. Equations (9) and (10) for the Onsager coefficients are then used instead of Eq. (17) together with the computed transport distribution (Fig. 2). The results are shown in Fig. 9. It is clear that the Lorenz factor can be significantly smaller than L_0 and takes a value around 2 at intermediate doping concentration. In fact using the metallic value L_0 in the determination of the lattice thermal conductivity leads to overestimation of the electronic thermal conductivity, and consequently to underestimation of the lattice contribution. Applying the computed L value corresponding to the real

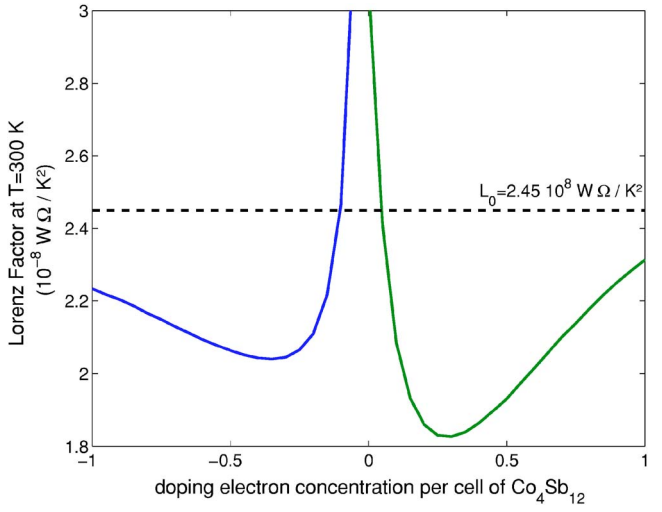

FIG. 9. (Color online) Calculated Lorenz factor at 300 K (negative values of doping are for holes and positive are for electrons).

TABLE I. Nominal composition versus the Hall number n_H (derived from experiments) and carrier concentration n per cell of Co_4Sb_{12} (used in calculations), where $n=n_H/\alpha$ with $\alpha\approx 1.1$ (see text). Note that the experimental Hall concentration for trivalent dopants markedly differs from the electron concentration expected from the nominal compositions.

Nominal composition	n_H	n	Ref.
$Tl_{0.1}Co_4Sb_{12}$	0.023	0.0209	30
$La_{0.05}Co_4Sb_{12}$	0.0631	0.0574	31
$Ce_{0.1}Co_4Sb_{12}$	0.1036	0.0909	5
$Nd_{0.05}Co_4Sb_{12}$	0.0096	0.0087	32
$Ni_{0.01}Co_{0.99}Sb_3$	0.04	0.0384	1
$Fe_{0.01}Co_{0.99}Sb_3$	0.04	0.0364[a]	1
$CoSb_3$		0.001	

[a]p doping.

doping concentration (instead of using $L_0=2.45\times10^{-8}$) could significantly improve the determination of κ_L.

C. Thermopower and conductivity

In this last part the calculations for thermopower and conductivity are presented and direct comparison with experimental measurement is obtained. The thermopower is independent of the relaxation time once τ is assumed to be constant. We can therefore compare our theoretical results to experimental data without adjustable parameters. On the other hand, the conductivity depends on τ which has to be adjusted to obtain the best fit to the experimental curves.

The calculation for S and σ has been performed using Eqs. (3) and (2) for different doping concentration corresponding to the experimental studies reported in Refs. 1, 5, and 30–32. Using Eqs. (14) and (15) in Eq. (3) we can note that the thermopower is proportional to the slope of the transport function ($S\propto a_\mu/b_\mu$).

In order to allow for coherent comparison between experimental data and computed results, we used the measured Hall concentration, instead of the nominal composition given in experimental work. Thus the concentration n used in our calculations was obtained from the experimental $n_H=1/R_Hq$ according to the results of Sec. IV A [$n=(1/\alpha)n_H$]. All these values are collected in Table I. It is noteworthy that one can observe an important difference between the nominal and Hall concentrations of electrons in the case of impurities filling the voids (La, Tl, Nd, and Ce), which may originate from the secondary phases observed in experimental work (e.g., Refs. 5 and 32). This approach also accounted for the difference in the calculated values for La- and Nd-doped samples, which have the same nominal concentration but very different n_H (Table I).

Once the value for n was determined, we obtained the chemical potential μ by solving the equation $n=\int^{\mu}f(E)g(E)dE$. S and σ were then computed by inserting μ into Eq. (9). The results of the thermopower calculations are presented in Fig. 10. The experimental measurements have been reproduced from Refs. 1, 5, and 30–32 and collected in Fig. 11. Bearing in mind the approximations that have been made (including the rigid-band approximation), we see that the agreement is quite satisfactory in all cases. The main difference corresponds to the kink in the experimental curve for iron-doped $CoSb_3$ for $T=600$ K, which is not found in the theoretical $S(T)$. Note, however, that other measurements for iron-doped $CoSb_3$ did not exhibit such temperature-dependent thermopower behavior.[33] Hence this discontinuity comes presumably from a change in the measurement technique at this temperature.

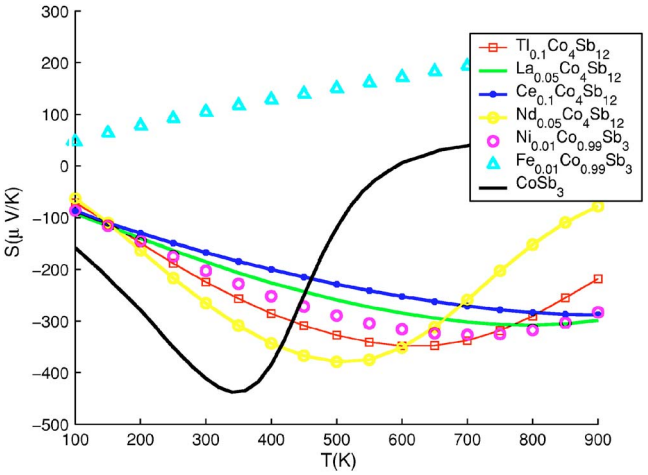

FIG. 10. (Color online) Calculated thermopower. The inset shows the nominal concentrations (according to Refs. 1, 5, and 30–32) but the carrier concentrations have been obtained from the Hall measurements (see Table I and related text). The compound noted as $CoSb_3$ corresponds to a slightly n-doped compound ($n=0.001$ electrons in the valence band).

To complete our electron transport property calculations we have investigated the dependence of the thermopower on the band-gap value and on the k dependence of the relaxation time. The upper panel in Fig. 12 shows the result of the calculations with a band gap which has been adjusted to the values found by Singh and Pickett[18] ($E_g=0.05$ eV) and to the

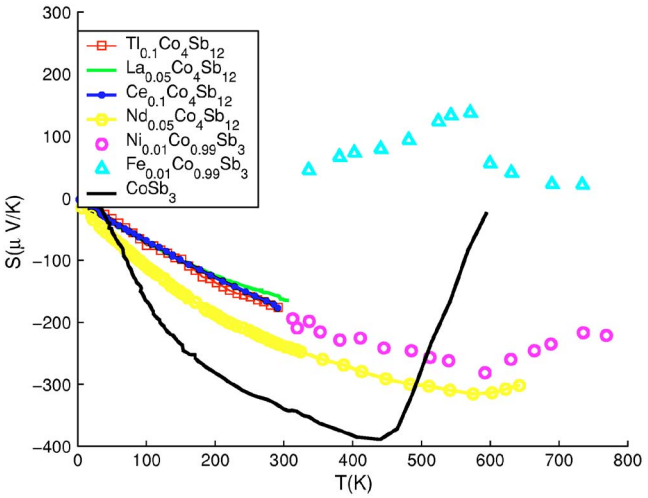

FIG. 11. (Color online) Experimental thermopower (from Refs. 1, 5, and 30–32).

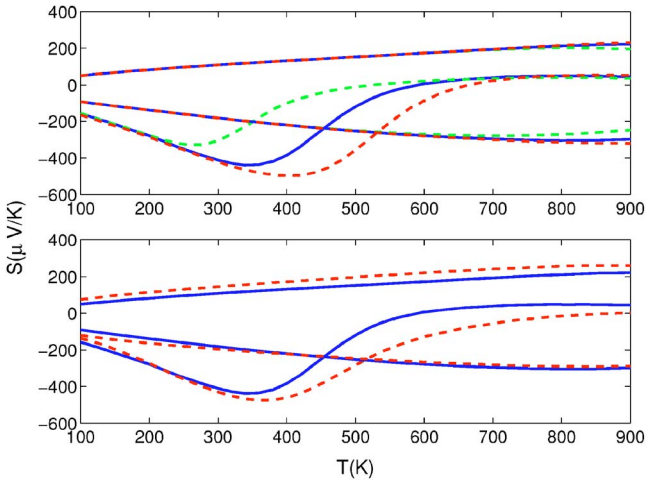

FIG. 12. (Color online) Calculated thermopower. In both panels the solid (blue) curves reproduce three selected cases (Fe- and La-doped and $CoSb_3$ skutterudites) from Fig. 10 with a constant relaxation time. In the lower panel the dashed (red) curves show the corresponding thermopower calculated with $\tau_k=\lambda_0/|\nabla E(k)|$. The upper panel compares the thermopower calculated with two different values of the band gap $E_g=0.05$ dashed (green) and 0.22 eV dashed (red) curves that are, respectively, above and below the solid (blue) curves.

value found by Sofo and Mahan[20] ($E_g=0.22$ eV) by shifting the conduction bands in a rigid way. The only significant differences are found at low doping concentration (noted as $CoSb_3$ in Figs. 10 and 11). At larger doping concentration corresponding to the case of physical interest, the differences are small since the compounds are nearly metallic and the precise gap value becomes unimportant.

The lower panel in Fig. 12 shows the results of the calculation performed with a k-dependent relaxation time $\tau_k=\lambda_0/|\nabla E_k|$ assuming a constant mean free path. Again at large doping concentration the differences are small. The curves for La- and Fe-doped skutterudites correspond, respectively, to the A and B ranges of Fig. 6. For higher n doping (region C) the difference between the constant-τ and k-dependent-τ results increases slightly, but for all doping it remains small.

Calculations have also been performed for the resistivity and the results for a constant relaxation time are presented in Fig. 13. The experimental curves are shown in Fig. 14. In Fig. 13 we have indicated the relaxation time chosen to get the best fit to the experimental curves under 300 K. These times are of order of 10^{-14} s. The conductivity is proportional to the relaxation time and the dependence on temperature from phonon scattering is not taken into account in the calculation. This may account for the difference with the experimental curves. However, Figs. 13 and 14 show that a large part of the temperature variation comes from the band structure and the Fermi factor.

The effect of the gap variation and the k dependence of the relaxation on the conductivity could also be discussed but the discussion is less meaningful because there is an adjustable parameter. For this reason we do not present the results in details but simply note that the behavior is the same as for the thermopower: the difference with the constant-relaxation-time approximation is only significant at very small doping concentration.

V. SUMMARY

We have presented the calculations for all the electron transport coefficients, the conductivity σ, the thermopower S, the Hall coefficient R_H, and the Lorentz factor L, in heavily doped $CoSb_3$ skutterudites. It was shown that there is only a small renormalization of the free-electron formula for the Hall coefficient. On the other hand the Lorenz factor L can significantly differ from the metallic value L_0 and we found a value around 2×10^{-8} W Ω/K^2 for current doping concentrations. The conductivity and the thermopower have also been calculated using the rigid-band approximation and a constant relaxation time. Quite good agreement was found between theoretical and experimental curves, which allows

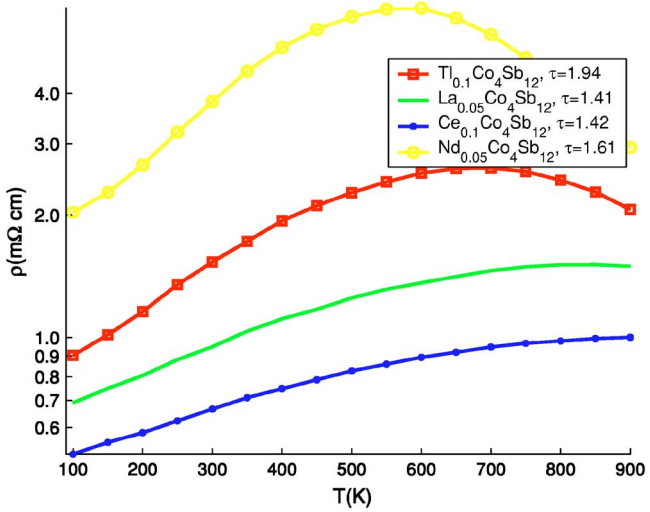

FIG. 13. (Color online) Calculated resistivity. The relaxation time τ is expressed in 10^{-14} s units.

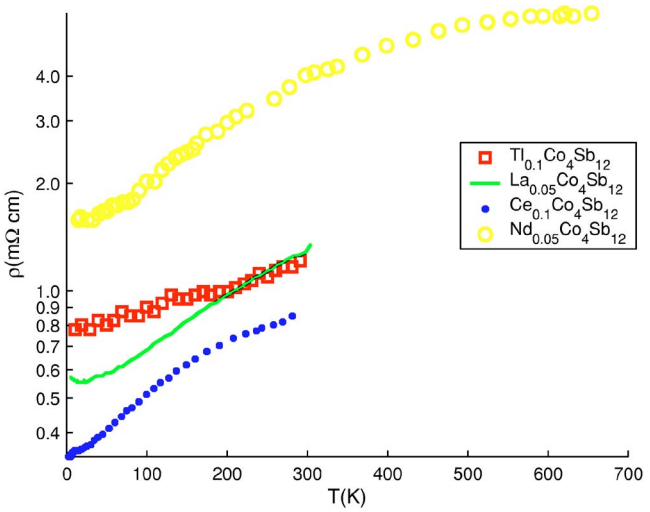

FIG. 14. (Color online) Experimental resistivity (from Refs. 5 and 30–32).

us to conclude that both used approximations are acceptable for heavily doped $CoSb_3$ materials. It is noteworthy that both approximations considerably simplify the calculations of transport properties and enable a theoretical search for good thermoelectric materials. In view of our theoretical study the large thermopower observed in skutterudites is mainly governed by the important slope of the transport function. Also the fact that the transport properties of doped skutterudites are well described using the electronic structure of the host material is in line with the PGEC concept.[3]

ACKNOWLEDGMENT

We want to thank Dr. V. L. Kuznetsov for providing resistivity and thermopower measurements for $Nd_xCo_4Sb_{12}$ in electronic form.[32]

APPENDIX: SPECTRAL DIFFERENTIATION

As output of band structure calculations, energies are only known on a discrete set of points in the first Brillouin zone. To calculate the electrons velocities these energies have to be differentiated in the reciprocal space according to $\vec{v}_k = (1/\hbar)\vec{\nabla}\epsilon_k$. In this Appendix we show how to calculate such a derivative. The method used is called spectral differentiation.

In the first part we present the one-dimensional case following Ref. 14. In the second part the method is generalized to any three-dimensional uniform set of grid points.

1. One-dimensional case: Notations

To fix the notations we first consider the one-dimensional case. Let v be a real periodic function, with period L, known at points x_i on a uniform grid $\{x_i = i(L/N), i = 0, \ldots, N\}$. For convenience we define $v_i = v(x_i)$ and $h = L/N$.

As usual, the discrete Fourier transform ($\mathcal{F}$) of the function v is defined as

$$\hat{v}_k = h\sum_{j=1}^{N} e^{ikx_j} v_j, \tag{A1}$$

where $k = (2\pi/Nh)p$, $p = -N/2+1, \ldots, N/2$ if N is even and $p = -(N-1)/2, \ldots, (N-1)/2$ if N is odd.

The reciprocal of Eq. (A1) is given by the inverse discrete Fourier transform ($\mathcal{I}$)

$$v_j = \frac{1}{L}\sum_{p} e^{i(2\pi/Nh)x_j p}\hat{v}_k, \quad j = 1, \ldots, N. \tag{A2}$$

Of course, the identity $\mathcal{I}(\mathcal{F}(v))|_{x_j} = v_j$ holds.

If x_j is extended to any $x \in]0, L]$, $x_j \to x$, Eq. (A2) can be seen to define an interpolation function $p(x)$. This is at the heart of spectral differentiation since the derivative of the function v at points x_j is then simply approximated by $w_i = p'(x_j)$. Formally, it is done in the following way.

First we write

$$v_j = \sum_{m=1}^{N} v_m \delta_{j-m}, \tag{A3}$$

where δ is the modulo N Kroenecker symbol.

Then using the identity $v_j = \mathcal{I}(\mathcal{F}(v))|_{x=x_j}$, Eq. (A3) becomes

$$\mathcal{I}(\mathcal{F}(v))|_{x=x_j} = \sum_{m=1}^{N} v_m \mathcal{I}(\mathcal{F}(\delta))|_{x=x_j - x_m}.$$

Evaluating both sides at the general position x instead of x_j we find

$$p(x) = \sum_{m=1}^{N} v_m S(x - x_m), \tag{A4}$$

where $S(x) = \mathcal{I}(\mathcal{F}(\delta))|_x$.

The reason for using the trick in Eq. (A3) is that the function $S(x)$ can be calculated exactly. In fact, using Eq. (A1), we find $\mathcal{F}(\delta) = h$.

So we simply get

$$S(x) = \frac{h}{L}\sum_{p} e^{i(2\pi/Nh)xp} = \frac{h}{L}\begin{cases} \cos\dfrac{\pi x}{Nh}\dfrac{\sin(\pi x/h)}{\sin(\pi x/Nh)} & \text{for } N \text{ even}, \\ \dfrac{\sin(\pi x/h)}{\sin(\pi x/Nh)} & \text{for } N \text{ odd}. \end{cases}$$

Finally the derivative at points x_j, $w_j = p'(x_j)$, are easily calculated from Eq. (A4) using

$$w_j = p(x_j) = \sum_{m=1}^{N} v_m S'(x_j - x_m) \tag{A5}$$

with

$$S'(x_j) = \begin{cases} \dfrac{\pi}{L}(-1)^j \cot\dfrac{\pi j}{N} & \text{for } N \text{ even}, \ j \neq 0 \bmod N, \\ \dfrac{\pi}{L}(-1)^j \dfrac{1}{\sin(\pi j/N)}, & \text{for } N \text{ odd}, \ j \neq 0 \bmod N, \\ 0 & \text{for } j = 0 \text{ and } N \text{ even or odd}. \end{cases}$$

The reliability of the method lies in the fact that energy bands (which are represented by v_j in the present case) are smooth functions. Their Fourier transforms are then rapidly decaying. Now from the Poisson summation formula

$$\hat{v}_k - \mathcal{F}[v](k) = \sum_{\substack{j=-\infty \\ j\neq 0}}^{\infty} \mathcal{F}[v]\left(k + \frac{2\pi j}{h}\right),$$

where $\mathcal{F}$ denotes the Fourier transform, it becomes clear that $\mathcal{F}$ and $\hat{v}_k$ get close when v is smooth. Using the Parseval identity, the same hold for the inverse Fourier transform of these quantities which are nothing but v and the interpolating

function $p(x)$. A more detailed discussion can be found in Ref. 14.

2. General case

The formalism of the preceding section can easily be generalized to the three-dimensional (3D) case.

To this end let us first rewrite Eq. (A5) in a matrix form:

$$\bar{w} = \bar{\bar{D}}\bar{v} \tag{A6}$$

where we have defined the row vectors $\bar{w}$ and $\bar{v}$ as

$$\bar{w} = [w_1 \cdots w_N]^T,$$

$$\bar{v} = [v_1 \cdots v_N]^T.$$

The matix $\bar{\bar{D}}$ is defined by its matrix elements

$$D_{ij} = S'(x_i - x_j). \tag{A7}$$

We now come to the calculation of the 3D derivative of the function v, i.e., the gradient vector $\vec{\nabla} v$. We assume the 3D space discretized uniformly along the lines spanned by the vectors $\mathbf{e}_1$, $\mathbf{e}_2$, $\mathbf{e}_3$,

$$x_1 = i_1 h_1, \quad i_1 = 1, \ldots, N_1,$$

$$x_2 = i_2 h_2, \quad i_2 = 1, \ldots, N_2,$$

$$x_3 = i_3 h_3, \quad i_3 = 1, \ldots, N_3.$$

Having in mind that the calculation for $\vec{\nabla} v$ will be implemented on a computer, we want to find an equation similar to Eq. (A6) for each component of the gradient vector. The differentiation matrices, say $\bar{\bar{D}}_1$, $\bar{\bar{D}}_2$, $\bar{\bar{D}}_3$ for each of the three directions, should also be as simple as possible.

In other words we should define a mapping $\{\mathbb{Z}^3 \mapsto \mathbb{Z}, (i_1, i_2, i_3) \to i\}$ which allows us to write $\bar{\bar{D}}_1$, $\bar{\bar{D}}_2$, $\bar{\bar{D}}_3$ in any case.

The most convenient choice is

$$i = i_3 + (i_2 - 1)N_3 + (i_1 - 1)N_2 N_3. \tag{A8}$$

Then it is easy to check that the covariant components of the gradient vector are given by

$$\bar{w}_1 = \bar{\bar{D}}_1 \bar{v},$$

$$\bar{w}_2 = \bar{\bar{D}}_2 \bar{v},$$

$$\bar{w}_3 = \bar{\bar{D}}_3 \bar{v},$$

with

$$\bar{\bar{D}}_1 = \bar{\bar{D}}(N_1) \otimes \bar{\bar{I}}(N_2) \otimes \bar{\bar{I}}(N_3),$$

$$\bar{\bar{D}}_2 = \bar{\bar{I}}(N_1) \otimes \bar{\bar{D}}(N_2) \otimes \bar{\bar{I}}(N_3),$$

$$\bar{\bar{D}}_3 = \bar{\bar{I}}(N_1) \otimes \bar{\bar{I}}(N_2) \otimes \bar{\bar{D}}(N_3).$$

$\bar{\bar{D}}(N)$ is the 1D differentiation matrix given by Eq. (A7) and $\bar{\bar{I}}(N)$ is the $N \times N$ identity matrix.

These equations show that the indexing in Eq. (A8) is the most convenient since instead of the large matrices $\bar{\bar{D}}_1$, $\bar{\bar{D}}_2$, $\bar{\bar{D}}_3$ the only things that have to be implemented are the small matrices $\bar{\bar{D}}(N_1)$, $\bar{\bar{D}}(N_2)$, $\bar{\bar{D}}(N_3)$. This saves a lot of computer memory.

[1] C. Uher, Semicond. Semimetals **69**, 139 (2001), and references therein.

[2] T. Caillat, A. Borshchevsky, and J. P. Fleurial, J. Appl. Phys. **80**, 4442 (1996).

[3] G. A. Slack, *Thermoelectric Handbook* (CRC Press, Boca Raton, FL, 1995).

[4] G. S. Nolas, M. Kaeser, R. T. Littleton IV, and T. M. Tritt, Appl. Phys. Lett. **77**, 1855 (2000).

[5] D. T. Morelli, G. P. Meisner, B. Chen, S. Hu, and C. Uher, Phys. Rev. B **56**, 7376 (1997).

[6] L. D. Chen, T. Kawahara, X. F. Tang, T. Goto, T. Hirai, J. S. Dyck, W. Chen, and C. Uher, J. Appl. Phys. **90**, 1864 (2001).

[7] J. S. Dyck, W. Chen, C. Uher, L. Chen, X. Tang, and T. Hirai, J. Appl. Phys. **91**, 3698 (2001).

[8] M. Puyet, B. Lenoir, A. Dauscher, M. Dehmas, C. Stiewe, and E. Müller, J. Appl. Phys. **95**, 4852 (2004).

[9] J. Yang, G. P. Meisner, D. T. Morelli, and C. Uher, Phys. Rev. B **63**, 014410 (2000).

[10] P. Blaha, K. Schwarz, G. K. H. Madsen, D. Kvasnicka, and J. Luitz, Computer code WIEN2K (Karlheinz Schwarz, Technical Universität, Wien, Austria, 2001).

[11] J. M. Ziman, *Electrons and Phonons* (Oxford University Press, Oxford, 1962).

[12] T. J. Scheidemantel, C. Ambrosch-Draxl, T. Thonhauser, J. V. Badding, and J. O. Sofo, Phys. Rev. B **68**, 125210 (2003).

[13] G. D. Mahan and J. O. Sofo, Proc. Natl. Acad. Sci. U.S.A. **93**, 7436 (1996).

[14] L. N. Trefethen, *Spectral Methods in Matlab* (SIAM, Philadelphia, 2000).

[15] N. P. Ong, Phys. Rev. B **43**, 193 (1991).

[16] W. W. Schulz, P. B. Allen, and N. Trivedi, Phys. Rev. B **45**, 10886 (1992).

[17] J. P. Perdew, K. Burke, and M. Ernzerhof, Phys. Rev. Lett. **77**, 3865 (1996).

[18] D. J. Singh and W. E. Pickett, Phys. Rev. B **50**, 11235 (1994).

[19] K. Koga, K. Akai, K. Oshiro, and M. Matsuura, Phys. Rev. B **71**, 155119 (2005).

[20] J. O. Sofo and G. D. Mahan, Phys. Rev. B **58**, 15620 (1998).

[21] E. Z. Kurmaev, A. Moewes, I. R. Shein, L. D. Finkelstein, A. L. Ivanovskii, and H. Anno, J. Phys.: Condens. Matter **16**, 979 (2004).

[22] P. Villars and L. D. Calvert, *Pearson's Handbook on Intermetallic Phases* (ASM International, Metals Park, OH, 1995).

[23] J. Tobola, K. Wojciechowski, J. Cieslak, and J. Leszczynsky, in

22nd International Conference on Thermoelectrics (IEEE, Piscataway, NJ, 2003), p. 76.
[24] S. Kaprzyk and A. Bansil, Phys. Rev. B **42**, 7358 (1990).
[25] A. Bansil, S. Kaprzyk, P. E. Mijnarends, and J. Tobola, Phys. Rev. B **60**, 13396 (1999).
[26] V. I. Anisimov, I. V. Solovyev, M. A. Korotin, M. T. Czyzyk, and G. A. Sawatzky, Phys. Rev. B **48**, 16929 (1993).
[27] P. Novak, computer code WIEN (2002).
[28] H. Harima and K. Takegahara, Physica B **312-313**, 843 (2003).
[29] F. J. Blatt, *Physics of Electronic Conduction in Solids* (McGraw-Hill, New York, 1968).
[30] B. C. Sales, B. C. Chakoumakos, and D. Mandrus, Phys. Rev. B **61**, 2475 (2000).
[31] G. S. Nolas, J. L. Cohn, and G. A. Slack, Phys. Rev. B **58**, 164 (1998).
[32] V. L. Kuznetsov, L. A. Kuznetsova, and D. M. Rowe, J. Phys.: Condens. Matter **15**, 5035 (2003).
[33] S. Katsuyama, Y. Shichijo, M. Ito, K. Majima, and H. Nagai, J. Appl. Phys. **84**, 6708 (1998).